

# Fake plunges are very eccentric real EMRIs in disguise

... they dominate the rates and are blissfully ignorant of angular momentum barriers

Pau Amaro-Seoane<sup>1,a</sup>, Carlos F. Sopuerta<sup>2,b</sup>, and Patrick Brem<sup>1,c</sup>

<sup>1</sup> Max-Planck Institut for Gravitational Physics (Albert Einstein-Institut)

<sup>2</sup> Institut de Ciències de l'Espai (CSIC-IEEC), Campus UAB, Torre C5 parells, 08193 Bellaterra, Spain

**Abstract.** The capture of a compact object in a galactic nucleus by a massive black hole (MBH) is the best way to map space and time around it. Compact objects such as stellar black holes on a capture orbit with a very high eccentricity have been wrongly assumed to be lost for the system after an intense burst of radiation, which has been described as a “direct plunge”. We prove that these very eccentric capture orbits spend actually a similar number of cycles in a LISA-like detector as those with lower eccentricities if the central MBH is spinning. Although the rates are higher for high-eccentricity EMRIs, the spin also enhances the rates of lower-eccentricity EMRIs. This last kind have received more attention because of the fact that high-eccentricity EMRIs were thought to be direct plunges and thus negligible. On the other hand, recent work on stellar dynamics has demonstrated that there seems to be a complot in phase space acting on these lower-eccentricity captures, since their rates decrease significantly by the presence of a blockade in the rate at which orbital angular momenta change takes place. This so-called “Schwarzschild barrier” is a result of the impact of relativistic precession on to the stellar potential torques, and thus it affects the enhancement on lower-eccentricity EMRIs that one would expect from resonant relaxation. We confirm and quantify the existence of this barrier using a statistical sample of 2,500 direct-summation  $N$ -body simulations using both a post-Newtonian but also, and for the first time, a geodesic approximation for the relativistic orbits. The existence of the barrier prevents “traditional EMRIs” from approaching the central MBH, but if the central MBH is spinning the rate will be anyway dominated by highly-eccentric extreme-mass ratio inspirals, which insolently ignore the presence of the barrier, because they are driven by two-body relaxation.

## 1 Introduction

One of the most exciting results of modern astronomy is the discovery, mostly through high-resolution observations of the kinematics of stars and gas, that most, if not all, nearby bright galaxies harbor a dark, massive, compact object at their centers. [1, 2]. The most spectacular case is our own galaxy, the Milky Way. By tracking and interpreting the stellar dynamics at the centre of our galaxy, we have the most well-established evidence for the existence of a massive black hole (MBH). The close examination of the Keplerian orbits of the so-called “S-stars” (also called S0-stars, where the letter S stands simply for source) has revealed the nature of the central dark object located at the Galactic Center. By following one of them, S2 (S02), the mass of SgrA\* was estimated to be about  $3.7 \times 10^6 M_{\odot}$  within a volume with radius no larger than 6.25 light-hours [3, 4]. More recent data based on 16 years of observations set the mass of the central MBH to  $\sim 4 \times 10^6 M_{\odot}$  [5, 6, 7, 8]. Observations of other galaxies indicate that the masses of MBH can reach a few billion solar masses. The existence of such a MBH population in the present-day universe is strongly supported by Sofian’s argument that the average mass density of these MBHs agrees with expectations from integrated luminosity of quasars [9, 10].

To interact closely with the central MBH, stars have to find themselves on “loss-cone” orbits, which are orbits elongated enough to have a very close-in pericenter [11, 12, 13]. The rate of tidal disruptions can be established (semi-)analytically if the phase space distribution of stars around the MBH is known [14, 15, 16] for estimates in models of observed nearby nuclei. To account for the complex influence of mass segregation, collisions and the evolution of the nucleus over billions of years, detailed numerical simulations are required, however [17, 18, 19, 20, 21, 22, 23, 24, 25].

Many correlations linking the MBH’s mass and overall properties of its host spheroid (bulge or elliptical galaxy) have been discovered. The tightest are with the spheroid mass [26], its velocity dispersion ( $M-\sigma$  relation, [27]) and degree of concentration [28]. Consequently, understanding the origin and evolution of these MBHs necessitates their study in the context of their surrounding stellar systems.

These observations are difficult, specially for low-mass MBH (ranging between  $10^5$  and  $10^7 M_{\odot}$ ) and more so for the even less-massive intermediate MBHs (IMBHs). Nowadays using adaptive optics we could optimistically hope to get a handful of measurements of stellar velocities of such targets about  $\sim 5$  kpc away in some ten years. Nevertheless, we need a bright reference star to guide us; the requirement of an astrometric reference system is crucial.

Therefore, in order to follow the same scheme of detection of inner stellar kinematics and of the masses of MBHs

<sup>a</sup> e-mail: Pau.Amaro-Seoane@aei.mpg.de

<sup>b</sup> e-mail: sopuerta@ieec.uab.es

<sup>c</sup> e-mail: Patrick.Brem@aei.mpg.de

in distant galaxies, we need the Very Large Telescope interferometer and one of the next-generation instruments, either the VSI or GRAVITY [29, 30]. Only then can we improve our astrometric accuracy by the necessary factor of  $\sim 10$ . This could allow us to follow the motion of stars orbiting a central MBH in a galaxy with the resolution we need to extract the mass of the black hole from the kinematics of the stars.

This is what makes an experiment such as eLISA [31, 32] so appealing from the viewpoint of an astrophysicist, since it can be envisaged as a magnifying glass that will look much deeper and with more detail in the areas of interest. However, this is only true for compact stars. Whilst main-sequence stars are tidally disrupted when approaching the central MBH, compact objects (stellar black holes, neutron stars, and white dwarfs) slowly spiral into the MBH and are swallowed after some  $\sim 10^5$  orbits in the eLISA band. At the closest approach to the MBH, the system emits a burst of GWs which contains information about the space-time geometry, the masses of the system, and the spins of the MBH. We can regard each such burst as a snapshot of the system. This is what makes EMRIs so appealing: a set of  $\sim 10^5$  bursts of GWs radiated by *one* system will tell us with the utmost accuracy about the system itself, it will test general relativity [33], it will tell us about the distribution of dark objects in galactic nuclei and globular clusters and, thus, we will have a new understanding of the physics of the process. Besides, new phenomena, unknown and unanticipated, are likely to be discovered.

On the other hand, this process is also directly linked to the growth of MBHs: Although there is an emerging consensus about the growth of large-mass MBHs thanks to Sołtan's argument, MBHs with masses up to  $10^7 M_\odot$ , such as our own MBH in the Galactic Centre (with a mass of  $\sim 4 \times 10^6 M_\odot$ ), are enigmatic. There are many different arguments to explain their masses: accretion of multiple stars from arbitrary directions [34], mergers of compact objects such as stellar-mass black holes and neutron stars [35] or IMBHs falling on to the MBH [36], or by more peculiar means such as accretion of dark matter [37] or collapse of supermassive stars [38, 39, 40, 41, 42]. Low-mass MBHs and, thus, the early growth of *all* MBHs, remain a conundrum.

eLISA is in this regard also attractive, for it will scrutinize exactly the range of masses fundamental to the understanding of the origin and growth of supermassive black holes. By extracting the information encoded in the GWs of this scenario, we can determine the mass of the central MBH with a ridiculous relative precision of  $\sim 10^{-4}$ . Additionally, the mass of the compact object which falls into the MBH and the eccentricity of the orbit will be recovered from the gravitational radiation with a fractional accuracy of also  $\sim 10^{-4}$ . All this means that eLISA will not be “just” the ultimate test of general relativity, but an exquisite probe of the spins and range of masses of interest for theoretical and observational astrophysics and cosmology.

## 2 Spinning MBHs

If the central MBH has a mass larger than  $10^7 M_\odot$ , then the signal of an inspiraling stellar black hole, even in its last stable orbit (LSO) will have a frequency too low for detection. On the other hand, if it is less massive than  $10^4 M_\odot$ ,

the signal will also be quite weak unless the source is very close. This is why one usually assumes that the mass range of MBHs of interest in the search of EMRIs for eLISA is between  $[10^7, 10^4] M_\odot$ . Nonetheless, if the MBH is rotating rapidly, then even if it has a mass larger than  $10^7 M_\odot$ , the LSO will be closer to the MBH and thus, even at a higher frequency, the system should be detectable. This would push the total mass to a few  $\sim 10^7 M_\odot$ .

For a binary of an MBH and a stellar black hole to be in the eLISA band, it has to have a frequency of between roughly  $10^{-4}$  and 1 Hz. The emission of GWs is more efficient as they approach the LSO, so that eLISA will detect the sources when they are close to the LSO line. The total mass required to observe systems with frequencies between  $10^{-4}$  and 1 Hz and is of  $10^4 - 10^7 M_\odot$ . For masses larger than  $10^7 M_\odot$  the frequencies close to the LSO will be too low, so that their detection will be very difficult. On the other hand, for a total mass of less than  $10^3 M_\odot$  we could in principal detect them at an early stage, but then the amplitude of the GWs would be rather low.

As the star spirals down towards the MBH, it has many opportunities to be deflected back by two-body encounters onto a “safer orbit” [43, 44], hence even the definition of a loss cone is not straightforward. Once again, the problem is compounded by the effects of mass segregation and resonant relaxation, to mention two main complications. As a result, considerable uncertainties are attached to the (semi-)analytical predictions of capture rates and orbital parameters of EMRIs.

Naively one could assume that the inspiral time is dominated by GW emission and that if this is shorter than a Hubble time, the compact object will become an EMRI. This is wrong, because one has to take into account the relaxation of the stellar system. Whilst it certainly can increase the eccentricity of the compact object, it can also perturb the orbit and circularize it, so that the required time to inspiral in,  $t_{\text{GW}}$ , becomes larger than a Hubble time. The condition for the small compact object to be an EMRI is that it is on an orbit for which  $t_{\text{GW}} \ll (1 - e)t_r$  [44], with  $t_r$  the *local* relaxation time. When the binary has a semi-major axis for which the condition is not fulfilled, the small compact object will have to be already on a so-called “plunging orbit”, with  $e \geq e_{\text{plunge}} \equiv 1 - 4R_{\text{Schw}}/a$ , where  $R_{\text{Schw}}$  is the Schwarzschild radius of the MBH, i.e.  $R_{\text{Schw}} = 2GM_\bullet/c^2$ , with  $M_\bullet$  being the MBH mass. It has been claimed a number of times by different authors that this would result in a too short burst of gravitational radiation which could only be detected if it was originated in our own Galactic Center [45] because one needs a coherent integration of some few thousands repeated passages through the periapsis in the eLISA bandwidth.

Therefore, such “plunging” objects would then be lost for the GW signal, since they would be plunging “directly” through the horizon of the MBH and only a final burst of GWs would be emitted, and such burst would be (i) very difficult to recover, since the very short signal would be buried in a sea of instrumental and confusion noise and (ii) the information contained in the signal would be practically nil. There has been some work on the detectability of such bursts [45, 46, 47], but they would only be detectable in our galaxy or in the close neighborhood, but the event rates are rather low, even in the most optimistic scenarios.

In figures 1 and 2 we show plots of the location of the LSO in the plane  $a$  (pc) -  $(1-e)$ , including the Schwarzschild separatrix between stable and unstable orbits,  $p-6-2e = 0$ , for both prograde and retrograde orbits and for different values of the inclination  $\iota$ . Each plot corresponds to a different value of the spin, showing how increasing the spin makes a difference in shifting the location of the separatrix between stable and unstable orbits, pushing prograde orbits near  $GM_\bullet/c^2$  while retrograde orbits are pushed out towards  $9GM_\bullet/c^2$ . The procedure we have used to build these plots is a standard one. Briefly, given a value of the dimensionless spin parameter  $s \equiv a_\bullet c^2/(GM_\bullet)$  and a value of the eccentricity  $e$  and inclination angle  $\iota$ , and we have followed the algorithm, definitions and notation introduced in [48].

In [48] it was estimated the number of cycles that certain EMRI orbital configurations that were thought to be plunging orbits (or orbits with no sufficient cycles) in the case of non-spinning MBHs can spend in a frequency regime of  $f \in [10^{-4}, 1]$  Hz during their last year(s) of inspiral before plunging into the MBH. This is important to assess how many of these EMRIs will have sufficient Signal-to-Noise Ratio (SNR) to be detectable. It was found that (prograde) EMRIs that are in a “plunge” orbit actually spend a significant number of cycles, more than sufficient to be detectable with good SNR. The number of cycles has been associated with  $N_\varphi$  (the number of times that the azimuthal angle  $\varphi$  advances  $2\pi$ ) which is usual for binary systems. However, as we have discussed above the structure of the waveforms from EMRIs is quite rich since they contain harmonics of three different frequencies. Therefore the waveforms have cycles associated with the three frequencies ( $f_r, f_\theta, f_\varphi$ ) which makes them quite complex and in principle this is good for detectability (assuming we have the correct waveform templates). Moreover, these cycles happen just before plunge and take place in the strong field region very near the MBH horizon. Then, these cycles should contribute more to the SNR than cycles taking place farther away from the MBH horizon.

We also estimate the impact on the event rates. Since “direct plunges” are actually diguesed EMRIs, although with a higher eccentricity. We prove that

$$\frac{a_{\text{EMRI}}^{\text{Kerr}}}{a_{\text{EMRI}}^{\text{Schw}}} = \mathcal{W}^{-\frac{5}{6-2\gamma}}(\iota, s) \quad (1)$$

$$\frac{\dot{N}_{\text{EMRI}}^{\text{Kerr}}}{\dot{N}_{\text{EMRI}}^{\text{Schw}}} = \mathcal{W}^{\frac{20\gamma-45}{12-4\gamma}}(\iota, s). \quad (2)$$

In the expression  $\mathcal{W}$  is a function that depends on  $\iota$ , the inclination of the EMRI and  $s$ , its spin<sup>1</sup>. We also have assumed that the SBHs distribute around the central MBH following a power-law cusp of exponent  $\gamma$ , i.e. that the density profile follows  $\rho \propto r^{-\gamma}$  within the region where the gravity of the MBH dominates the gravity of the stars, with  $\gamma$  ranging between 1.75 and 2 for the heavy stellar components [24, 25, 49, 50, 51, 52, 53, 54] and see [55] for an interesting first idea of this concept<sup>2</sup>.

<sup>1</sup> For the derivation and some examples of values for  $\mathcal{W}$ , we refer the reader to the work of [48].

<sup>2</sup> The authors obtained a similar solution for how electrons distribute around a positively charged Coulomb centre.

For instance, for a spin of  $s = 0.999$  and an inclination of  $\iota = 0.4$  rad, we estimate that  $\mathcal{W} \sim 0.26$  and, thus,  $\dot{N}_{\text{EMRI}}^{\text{Kerr}} \sim 30$ . I.e. *we boost the event rates by a factor of 30* in comparison to a non-rotating MBH.

### 3 Analysing a blockade in angular momentum for low-eccentricity EMRIs with a direct-summation $N$ -body sample of 2,500 simulations

In a gravitational potential with a high degree of symmetry, a test star will receive gravitational tugs from the rest of the field stars which are not totally arbitrary and hence do not add up in a random walk way, but *coherently*. The potential will prevent stellar orbits from evolving in an erratic way. In a two-body Keplerian system, a stellar-mass black hole will orbit around the MBH in a fixed ellipse. The stellar BH will not feel random gravitational tugs. It evolves coherently as the result of the action of the gravitational potential. When an EMRI approaches the periapsis of its orbit, we can envisage the situation as a pure two-body problem; initially Newtonian but later GR effects must be taken into account as the periapsis grows smaller and smaller. Nonetheless, as the stellar BH goes back to the apoapsis, it will feel the surrounding stellar system, distributed in the shape of a cusp which grows in mass the further away we are from the periapsis. The time spent in the region in which we can regard this as a two-body problem is much shorter than the time in which the stellar BH will feel the rest of the stellar system. This is particularly true for the kind of objects of our interest, since the very high eccentricity implies a large semi-major axis. The time spent on periapsis is negligible as compared with the time spent on apoapsis. In that region, the stellar BH feels the graininess of the potential. The gravitational tugs from other stars will alter its orbit. The mean free path in  $J$ -space of that test stellar BH is very large and thus, it has a *fast* random walk. Both the magnitude and direction of  $J$  of the stellar black hole are altered. When the modulus is changed but not the direction, we talk of “scalar” resonant relaxation, and correspondingly when the direction is changed but not the modulus, “vector” resonant relaxation.

In particular, in the potential of a point mass, orbits are frozen fixed ellipses that exert a continuous torque on the test star. A test star does not feel random kicks from all directions. When we add up the individual contributions coming from all the rest of the stars on the test star, there is a residual, non-negligible torque that will influence its evolution. The mean free path of the star in  $J$  space is very large. We will refer to this phenomenon as *scalar* resonant (or coherent) relaxation, because it can change both the magnitude of  $J$  and the inclination of the orbital plane of the test star. In this scenario it is possible to alter an initially very circular orbit and modify it in such a way that the test star will get very close to the MBH after the torques have acted. i.e., we open a new window for stars to fall into a capture orbit that will lead to an EMRI.

The impact of coherent relaxation on the production of EMRIs is important. While the underlying physics of the process is very robust, it is a rather difficult task to assign values to the different parameters on which the process depends. A possible way of assigning these was sug-

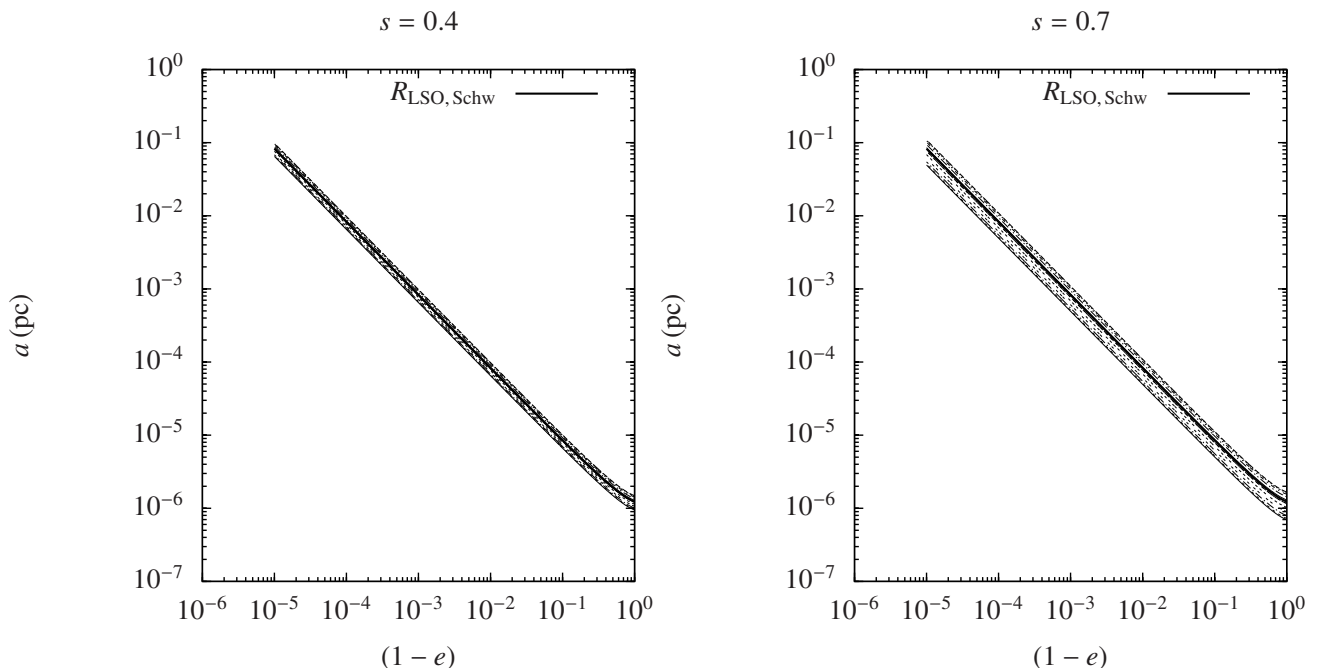


**Fig. 1.** LSO for a MBH of mass  $4 \times 10^4 M_\odot$  and a SBH of mass  $m_\bullet = 10 M_\odot$  for a Kerr MBH of spin  $s = 0.4$  (left) and  $s = 0.7$  (right). The Schwarzschild separatrix is given as a solid black line. Curves above it correspond to retrograde orbits and inclinations of  $\iota = 5.72, 22.91, 40.10, 57.29, 74.48$  and  $89.95^\circ$  starting from the last value ( $89.95^\circ$ ). In the left panel we can barely see any difference from the different inclinations due to the low value of the spin.

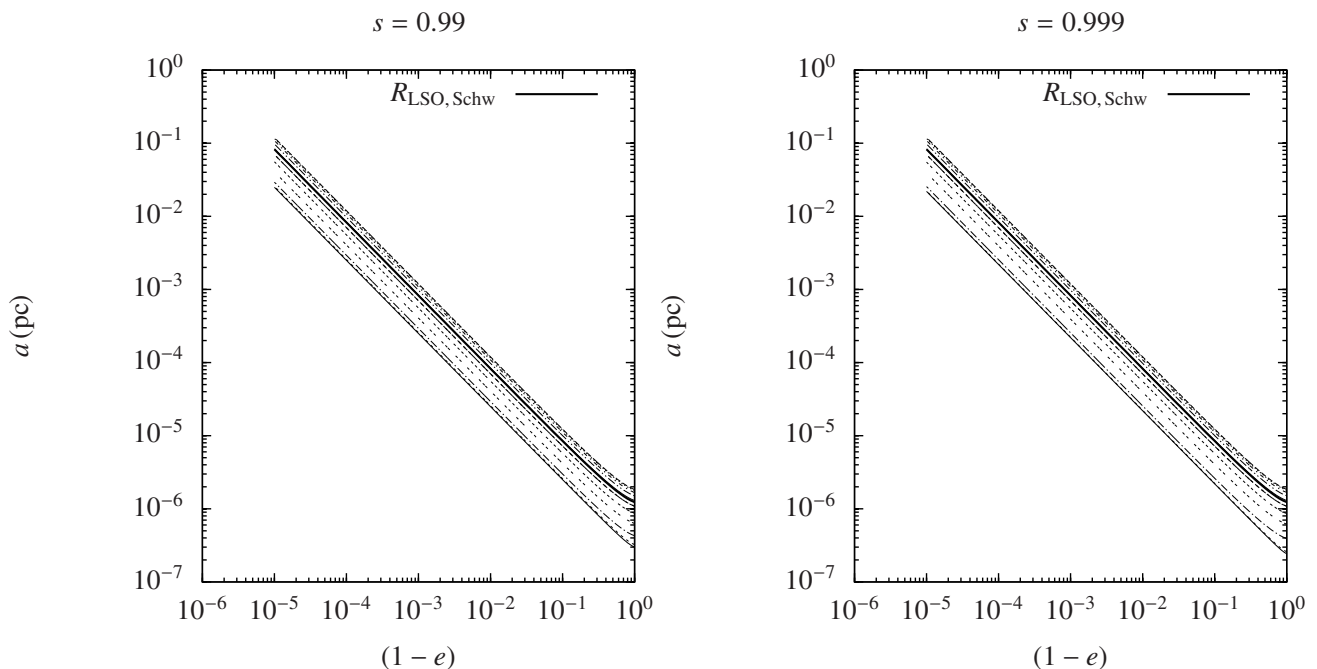


**Fig. 2.** As in figure 1 but for a spin of  $s = 0.99$  (left) and  $s = 0.999$  (right panel). The larger the spin, the “further away” the Kerr LSO gets from the Schwarzschild LSO.

gested in [56, 57]. In Figure 6 of [57], they show the rate of EMRIs and plunges in a system in which we take into account both orthodox or regular relaxation and coherent relaxation, normalised to what one can expect when only taking into account normal relaxation. The numerical simulations of [57] show that coherent relaxation can enhance the EMRI rate by a factor of a few over the rates predicted assuming only slow stochastic two-body relaxation.

Recently, [58] estimated with a few direct-summation  $N$ -body simulations expanded with a statistical Monte-

Carlo study that the production of “traditional EMRIs” via resonant relaxation is markedly decreased by the presence of a blockade in the rate at which orbital angular momenta change takes place. This so-called “Schwarzschild barrier” is a result of the impact of relativistic precession on to the stellar torques. Although the authors find that some particles can penetrate the barrier, EMRIs are significantly suppressed in this scenario.

We have felt motivated by these results and recently decided to study the effect with a set of *some 2,500* direct-

summation  $N$ -body simulations, including post-Newtonian corrections and also, for the first time, the implementation of a solver of geodesic equations in the same code [59]. For this, we use a modification of the publicly available `planet` code by Sverre Aarseth, a direct summation  $N$ -Body integrator [60, 61]. For our study we use several different methods to account for the general relativistic corrections of the Newtonian accelerations:

- purely Newtonian
- post-Newtonian (PN) corrections
- geodesic equations

In the purely Newtonian case, the integration is done without modifications to the acceleration equations. In the PN case we add PN corrections in the following way:

$$F = \underbrace{F_0}_{\text{Newt.}} + \underbrace{c^{-2}F_2}_{\text{1PN}} + \underbrace{c^{-4}F_4}_{\text{2PN}} + \underbrace{c^{-5}F_5}_{\text{2.5PN}} + \underbrace{\mathcal{O}(c^{-6})}_{\text{neglected}}, \quad (3)$$

i.e., as described in the pioneering work of [62]. The individual  $F_i$  can be found in [63], their equation (7.16).

Given the high mass ratio for EMRIs, their motion around a MBH can also be approximated by solving the geodesic equations. These equations give the exact trajectory of a test mass particle around a Schwarzschild BH. Unlike the PN approximation, the geodesic equations are valid even in the last few  $r_g$  during a plunge or inspiral, however only in the limit  $m_*/M_\bullet \rightarrow 0$ . Some orbits are expected to migrate towards plunge or inspiral orbits at pericenter distances of  $r_p < 15 r_g$ , where the errors of the PN approximation can already be quite significant [64]. In order to test the existence of the Schwarzschild barrier at small distances, we implemented these corrections in the `planet` code.

Although we confirm the blockade, we note that the systems the two groups study are representative but artificial, because they integrate only 50 particles with the same mass distributed around the MBH. In this regard, the existence of this quenching must be still explored in more detail, in particular with direct-summation simulations with realistic number of stars and mass ranges.

In any case, in this scenario the barrier can roughly be fitted in  $a - e$  space as

$$a_{\text{SB}} \approx C_{\text{SB}} \cdot (1 - e^2)^{-1/3}. \quad (4)$$

In the last equation  $a_{\text{SB}}$  is the semi-major axis in mpc below which penetration of particles is severely suppressed and  $C_{\text{SB}}$  is a constant of order unity. [58] choose  $C_{\text{SB}} = 0.7$ . We depict the barrier in figure 6. As we can see, and as described in the work of [58], the barrier poses a real problem for stars with small semi-major axis, and below it, the evolution is dominated by two-body relaxation.

In order to quantify the nature of the ‘‘Schwarzschild barrier’’, we first plot the normalized presence density as a histogram in the  $(a, 1 - e)$  plane for the Newtonian case, Fig. 4 (left panel) and the relativistic case (right panel), and we give the theoretical distribution in figure 3. If we consider our specific setup, there are 3 different regions in the  $(a, 1 - e)$  plane where different mechanisms are efficient. In the right-most region, where pericenters are large, RR plays the dominant role. The left border of this region is

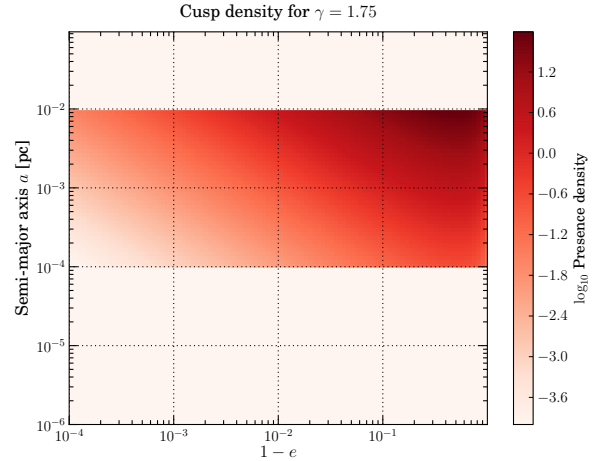


**Fig. 3.** Theoretical distribution for the density of presence of a cusp of power-law 1.75 around a MBH, using a truncated distribution.

roughly given by the appearance of the Schwarzschild precession which inhibits the BHs from experiencing coherent torques [59]. We derive that  $C_{\text{SB}} = 0.35$ .

## 4 Only fake plunges survive: Real EMRIs

For a fast spinning MBH, the separatrix for prograde orbits is shifted to significantly lower  $a$  values, with a corresponding higher value of the critical semi-major axis, corresponding to the point PP in figure 6. As we have explained above, it is this effect which can lead to a significant increase in the EMRI rate, combined with the fact that the critical point for retrograde orbits (PR) is much less affected and that an isotropic orbit distribution is expected, thanks to relaxational processes. However this increase in EMRI rate would can be thwarted by vector RR if this process can change the orbital orientation of a SBH after it has crossed the ‘‘ $t_{\text{GW}} = t_{\text{r,peri}}$ ’’ line and before it has completed its GW-driven inspiral, i.e. on a timescale shorter than  $t_{\text{GW}}$ . Indeed, if the orbit becomes significantly less prograde as the the inspiral takes place, due to RR, the separatrix moves up and the SBH might suddenly find itself on a plunge orbit.

To check for this possibility, we also plot, in figure 6, a long-dashed line corresponding to the condition  $t_{\text{GW}} = t_{\text{RR,v}}$ , with  $t_{\text{GW}} < t_{\text{RR,v}}$  on the left of this line. SBHs that cross the ‘‘ $t_{\text{GW}} = t_{\text{r,peri}}$ ’’ line while on the left side of the ‘‘ $t_{\text{GW}} = t_{\text{RR,v}}$ ’’ line keep their orbital orientation during their inspiral and complete it without abrupt plunge. One can see that, for our choice of parameters, this is the case for all prograde orbits. On the other hand, retrograde orbits can cross the ‘‘ $t_{\text{GW}} = t_{\text{r,peri}}$ ’’ line while RR is still effective enough to change their orientation during inspiral. However, the effect of RR on retrograde orbits cannot reduce significantly the total EMRI rate and may even increase it slightly because (1) these orbits contribute less than the prograde ones (and more to the plunge rate) and (2) statistically, RR is more likely to make the orbit become less retrograde which pushes down the separatrix.

Moreover, as we can see in figure 6, for semi-major axis with values approximately  $a \gtrsim 0.03$  pc, the barrier lies well below the last separatrix, and so EMRIs originating

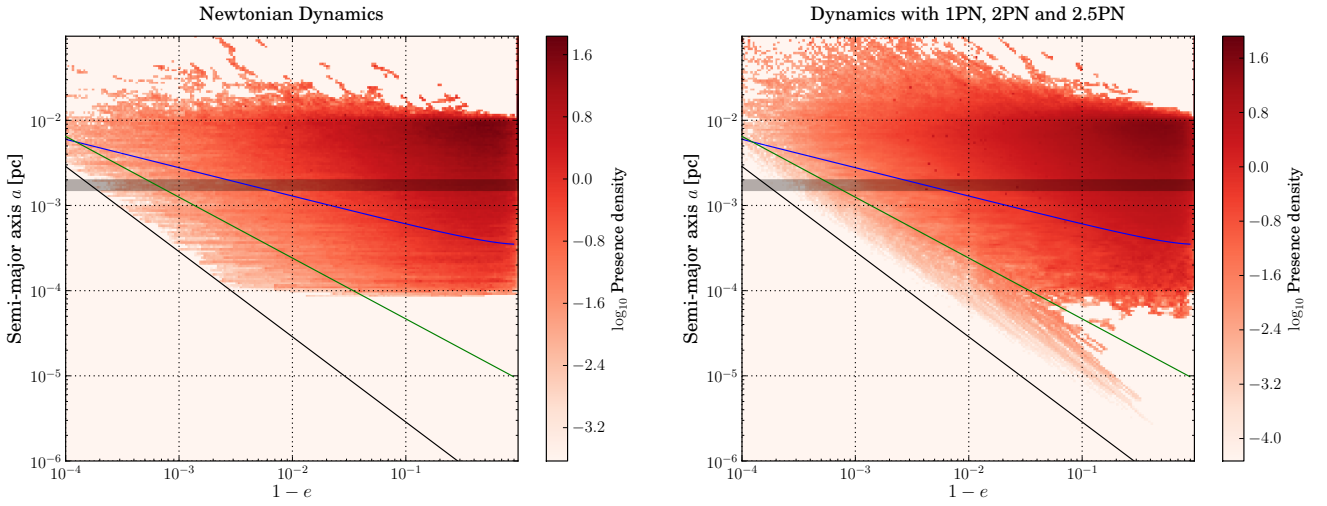


**Fig. 4.** Integrated presence density for the Newtonian (left panel) and the relativistic case (right panel). The shaded box marks the region of the slice analyzed in Fig. 5. The lines indicate the position of the Schwarzschild barrier with  $C_{SB} = 0.35$  (blue) and the limit for capture onto inspiral orbits for non-resonant relaxation (green).

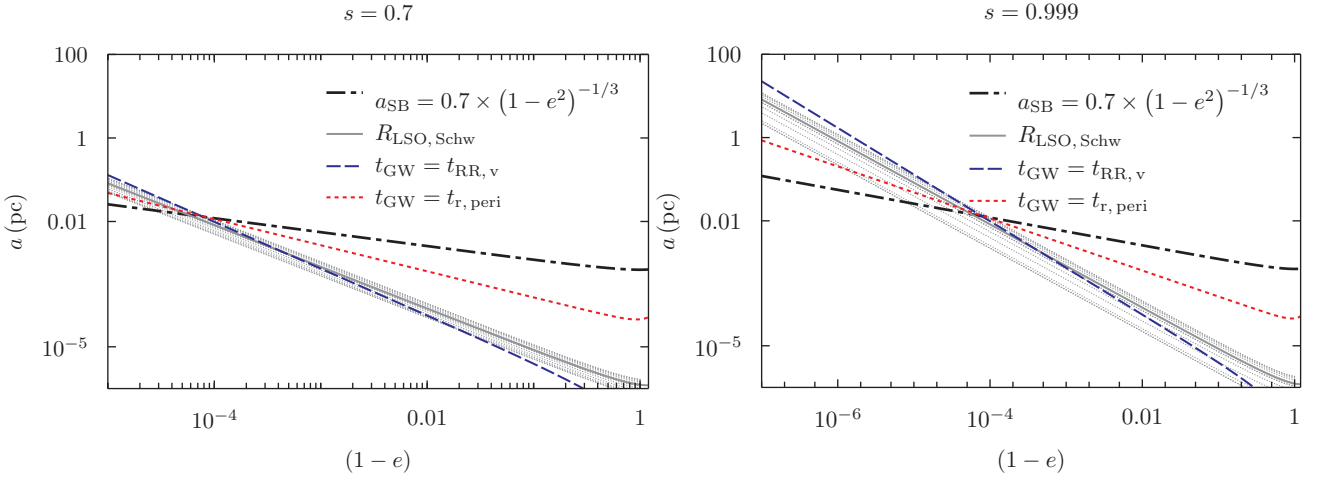


**Fig. 6.** *Left panel:* Relation between different timescales in the  $s = 0.7$  case. We display the Schwarzschild separatrix as a solid, black line and the separatrices for different inclinations with different curves in light grey. The dashed, blue line shows the value of  $a$  and  $1 - e$  for which the vectorial resonant relaxation timescale ( $t_{RR, v}$ ) is equal to the gravitational loss timescale ( $t_{GW}$ ). The dashed, dotted line corresponds to the values of  $a$  and  $1 - e$  for which the relaxation time at periastris ( $t_{r, peri}$ ) equals the gravitational loss timescale. The dashed-dotted, black curve describes the “Schwarzschild barrier”. *Right panel:* Same as the left panel but for a spin value of  $s = 0.999$ .

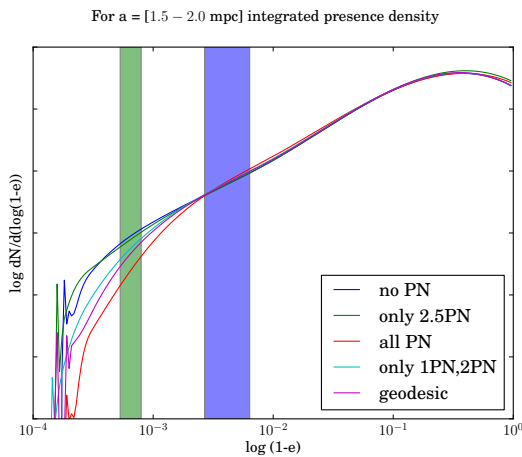


**Fig. 5.** Integrated presence density for a semi-major axis slice  $1.5 \text{ mpc} < a < 2.0 \text{ mpc}$ . The shaded boxes represent the position of the Schwarzschild barrier with  $C_{SB} = 0.35$  (blue) and the limit for capture on to inspiral orbits for non-resonant relaxation (green).

from these area, the “plunges” we have discussed in this work, will not suffer this quenching in phase space.

## 5 Conclusions

The event rate of “plunges” is much larger than that of EMRIs, as a number of different studies by different authors using different methods find. Up to now spin effects of the central MBH have been always ignored. Hence, the question arises, whether a plunge is really a plunge when the central MBH is spinning. This consideration has been so far always ignored.

So as to estimate EMRI event rates, one needs to know whether the orbital configuration of the compact object is stable or not, because this is the kernel of the difference between an EMRI and a plunge. In this paper we take into account the fact that the spin makes the LSO to be much closer to the horizon in the case of prograde orbits but it pushes it away for retrograde orbits. Since the modifica-

tions introduced by the spin are not symmetric with respect to the non-spinning case, and they are more dramatic for prograde orbits, we prove that the inclusion of spin increases the number of EMRI events by a significant factor. The exact factor of this enhancement depends on the spin, but the effect is already quite important for spins around  $s \sim 0.7$ .

We also prove that these fake plunges, “our” EMRIs, do spend enough cycles inside the band of eLISA to be detectable, i.e. they are to be envisaged as typical EMRIs. We note here that whilst it is true that EMRIs very near the new separatrix shifted by the spin effect will probably contribute not enough cycles to be detected, it is equally true for the old separatrix (Schwarzschild, without spin). In this sense, we find that the spin increases generically the number of cycles inside the band for prograde EMRIs in such a way that EMRIs very near to the non-spin separatrix, which contributed few cycles, become detectable EMRIs. In summary, spin increases the area, in configuration space of detectable EMRIs. We predict thus that EMRIs will be highly dominated by prograde orbits.

We also demonstrate that these new kind of EMRIs we describe here originate in a region of phase-space such that they will be ignorant of the Schwarzschild barrier. The reason for that is that they are driven by two-body relaxation and not resonant relaxation. While the boost in EMRI rates due to resonant relaxation is affected by the Schwarzschild barrier, so that “standard” EMRIs run into the problem of having to find a way to cross it, our “plunge-EMRIs” are already in the right place and led by two-body relaxation. The barrier affects the productions of EMRIs via torques, but not two-body relaxation, which is the mechanism producing the “plunge-EMRIs”. Moreover, because the suppression in the rates is severe for those EMRIs with semi-major axis with values approximately  $a \gtrsim 0.03$  pc, we predict that the rates will be dominated by the kind of EMRIs we have described in this work.

## Acknowledgments

PAS is indebted with S. Komossa and R. Saxton for asking him to give an invited talk at the The Tidal Disruption Workshop. This work has been supported by the Transregio 7 “Gravitational Wave Astronomy” financed by the Deutsche Forschungsgemeinschaft DFG (German Research Foundation). CFS acknowledges support from the Ramón y Cajal Programme of the Spanish Ministry of Education and Science, contract 2009-SGR-935 of AGAUR, and contracts FIS2008-06078-C03-03, AYA-2010-15709, and FIS2011-30145-C03-03 of MICCIN. We acknowledge the computational resources provided by the BSC-CNS (AECT-2011-3-0007) and CESGA (contracts CESGA-ICTS-200 and CESGA-28-ICTS-221).

## References

1. L. Ferrarese, H. Ford, *Supermassive Black Holes in Galactic Nuclei: Past, Present and Future Research* (2005)
2. J. Kormendy, *The Stellar-Dynamical Search for Supermassive Black Holes in Galactic Nuclei*, in *Coevolution of Black Holes and Galaxies, from the Carnegie Observatories Centennial Symposia.*, edited by L. Ho (Cambridge University Press, 2004), p. 1
3. R. Schödel, T. Ott, R. Genzel, A. Eckart, N. Mouawad, T. Alexander, *ApJ* **596**, 1015 (2003), [arXiv:astro-ph/0306214](#)
4. A.M. Ghez, G. Duchêne, K. Matthews, S.D. Hornstein, A. Tanner, J. Larkin, M. Morris, E.E. Becklin, S. Salim, T. Kremenek et al., *ApJ Lett.* **586**, L127 (2003), [arXiv:astro-ph/0302299](#)
5. F. Eisenhauer, R. Genzel, T. Alexander, R. Abuter, T. Paumard, T. Ott, A. Gilbert, S. Gillessen, M. Horrobin, S. Trippe et al., *ApJ* **628**, 246 (2005), [arXiv:astro-ph/0502129](#)
6. A.M. Ghez, S. Salim, S.D. Hornstein, A. Tanner, J.R. Lu, M. Morris, E.E. Becklin, G. Duchêne, *ApJ* **620**, 744 (2005)
7. A.M. Ghez, S. Salim, N.N. Weinberg, J.R. Lu, T. Do, J.K. Dunn, K. Matthews, M.R. Morris, S. Yelda, E.E. Becklin et al., *ApJ* **689**, 1044 (2008), [0808.2870](#)
8. S. Gillessen, F. Eisenhauer, S. Trippe, T. Alexander, R. Genzel, F. Martins, T. Ott, *ApJ* **692**, 1075 (2009), [0810.4674](#)
9. A. Softan, *MNRAS* **200**, 115 (1982)
10. Q. Yu, S. Tremaine, *MNRAS* **335**, 965 (2002)
11. J. Frank, M.J. Rees, *MNRAS* **176**, 633 (1976)
12. A.P. Lightman, S.L. Shapiro, *ApJ* **211**, 244 (1977)
13. P. Amaro-Seoane, R. Spurzem, *MNRAS* **327**, 995 (2001)
14. J. Magorrian, S. Tremaine, *MNRAS* **309**, 447 (1999)
15. D. Syer, A. Ulmer, *MNRAS* **306**, 35 (1999)
16. J. Wang, D. Merritt, *ApJ* **600**, 149 (2004)
17. L.P. David, R.H. Durisen, H.N. Cohn, *ApJ* **313**, 556 (1987)
18. L.P. David, R.H. Durisen, H.N. Cohn, *ApJ* **316**, 505 (1987)
19. B.W. Murphy, H.N. Cohn, R.H. Durisen, *ApJ* **370**, 60 (1991)
20. M. Freitag, W. Benz, *A&A* **394**, 345 (2002)
21. H. Baumgardt, J. Makino, T. Ebisuzaki, *ApJ* **613**, 1143 (2004)
22. M. Freitag, P. Amaro-Seoane, V. Kalogera, *ApJ* **649**, 91 (2006), [arXiv:astro-ph/0603280](#)
23. E. Khalisi, P. Amaro-Seoane, R. Spurzem, *MNRAS* (2007), [arXiv:astro-ph/0602570](#)
24. M. Preto, P. Amaro-Seoane, *ApJ Lett.* **708**, L42 (2010), [0910.3206](#)
25. P. Amaro-Seoane, M. Preto, *Classical and Quantum Gravity* **28**, 094017 (2011), [1010.5781](#)
26. N. Häring, H.W. Rix, *ApJ Lett.* **604**, L89 (2004)
27. S. Tremaine, K. Gebhardt, R. Bender, G. Bower, A. Dressler, S.M. Faber, A.V. Filippenko, R. Green, C. Grillmair, L.C. Ho et al., *ApJ* **574**, 740 (2002)
28. P. Erwin, A.W. Graham, N. Caon, *The Correlation between Supermassive Black Hole Mass and the Structure of Ellipticals and Bulges*, in *Coevolution of Black Holes and Galaxies*, edited by L. C. Ho (2004)
29. S. Gillessen, G. Perrin, W. Brandner, C. Straubmeier, F. Eisenhauer, S. Rabien, A. Eckart, P. Lena, R. Genzel, T. Paumard et al., *GRAVITY: the adaptive-optics-assisted two-object beam combiner instrument for the VLTI*, in *Society of Photo-Optical Instrumentation Engineers (SPIE) Conference Series* (2006), Vol. 6268 of *Society of Photo-Optical Instrumentation Engineers*

- (SPIE) Conference Series
30. F. Eisenhauer, G. Perrin, W. Brandner, C. Straubmeier, A. Richichi, S. Gillessen, J.P. Berger, S. Hippler, A. Eckart, M. Schöller et al., *GRAVITY: getting to the event horizon of Sgr A\**, in *Society of Photo-Optical Instrumentation Engineers (SPIE) Conference Series* (2008), Vol. 7013 of *Society of Photo-Optical Instrumentation Engineers (SPIE) Conference Series*
  31. P. Amaro-Seoane, S. Aoudia, S. Babak, P. Binétruy, E. Berti, A. Bohé, C. Caprini, M. Colpi, N.J. Cornish, K. Danzmann et al., Accepted for publication at *GW Notes* (2012), 1201.3621
  32. P. Amaro-Seoane, S. Aoudia, S. Babak, P. Binétruy, E. Berti, A. Bohé, C. Caprini, M. Colpi, N.J. Cornish, K. Danzmann et al., *Classical and Quantum Gravity* **29**, 124016 (2012), 1202.0839
  33. C.F. Sopuerta, *GW Notes*, Vol. 4, p. 3-47 **4**, 3 (2010)
  34. J.G. Hills, *Nat* **254**, 295 (1975)
  35. G.D. Quinlan, S.L. Shapiro, *ApJ* **356**, 483 (1990)
  36. S.F. Portegies Zwart, H. Baumgardt, S.L.W. McMillan, J. Makino, P. Hut, T. Ebisuzaki, *ApJ* **641**, 319 (2006), arXiv:astro-ph/0511397
  37. J.P. Ostriker, *Physical Review Letters* **84**, 5258 (2000), arXiv:astro-ph/9912548
  38. T. Hara, *Progress of Th. Phys.* **60**, 711 (1978)
  39. S.L. Shapiro, S.A. Teukolsky, *ApJ Lett.* **234**, L177 (1979)
  40. M.J. Rees, *ARA&A* **22**, 471 (1984)
  41. P. Amaro-Seoane, Ph.D. thesis, PhD Thesis, Combined Faculties for the Natural Sciences and for Mathematics of the University of Heidelberg, Germany. VII + 174 pp. (2004), <http://www.ub.uni-heidelberg.de/archiv/4826> (2004)
  42. M.C. Begelman, *MNRAS* **402**, 673 (2010), 0910.4398
  43. T. Alexander, C. Hopman, *ApJ Lett.* **590**, 29 (2003)
  44. P. Amaro-Seoane, J.R. Gair, M. Freitag, M.C. Miller, I. Mandel, C.J. Cutler, S. Babak, *Classical and Quantum Gravity* **24**, 113 (2007), arXiv:astro-ph/0703495
  45. C. Hopman, M. Freitag, S.L. Larson, *MNRAS* **378**, 129 (2007), arXiv:astro-ph/0612337
  46. L.J. Rubbo, K. Holley-Bockelmann, L.S. Finn, *ApJ Lett.* **649**, L25 (2006)
  47. N. Yunes, C.F. Sopuerta, L.J. Rubbo, K. Holley-Bockelmann, *ApJ* **675**, 604 (2008), 0704.2612
  48. P. Amaro-Seoane, C.F. Sopuerta, M. Dewi Freitag, *ArXiv e-prints* (2012), 1205.4713
  49. P.J.E. Peebles, *ApJ* **178**, 371 (1972)
  50. J.N. Bahcall, R.A. Wolf, *ApJ* **209**, 214 (1976)
  51. J.N. Bahcall, R.A. Wolf, *ApJ* **216**, 883 (1977)
  52. P. Amaro-Seoane, M. Freitag, R. Spurzem, *MNRAS* (2004), astro-ph/0401163
  53. M. Preto, D. Merritt, R. Spurzem, *ApJ Lett.* **613**, L109 (2004)
  54. T. Alexander, C. Hopman, *ApJ* **697**, 1861 (2009)
  55. A. Gurevich, *Geomag. Aeronom.* **4**, 247 (1964)
  56. C. Hopman, T. Alexander, *ApJ* **645**, 1152 (2006), arXiv:astro-ph/0601161
  57. E. Eilon, G. Kupi, T. Alexander, *ApJ* **698**, 641 (2009), 0807.1430
  58. D. Merritt, T. Alexander, S. Mikkola, C.M. Will, *Phys. Rev. D* **84**, 044024 (2011), 1102.3180
  59. P. Brem, P. Amaro-Seoane, C. Sopuerta, Submitted to *MNRAS* (2012)
  60. S.J. Aarseth, *The Publications of the Astronomical Society of the Pacific* **111**, 1333 (1999)
  61. S.J. Aarseth, *Gravitational N-Body Simulations* (ISBN 0521432723. Cambridge, UK: Cambridge University Press, November 2003., 2003)
  62. G. Kupi, P. Amaro-Seoane, R. Spurzem, *MNRAS* pp. L77+ (2006), astro-ph/0602125
  63. L. Blanchet, G. Faye, *Phys. Rev. D* **63**, 062005 (2001), arXiv:gr-qc/0007051
  64. N. Yunes, E. Berti, *Ph. Rv. D* **77**, 124006 (2008), 0803.1853